Advanced Journal of Physical Sciences
Volume 2(1), pages 1-11
February, 2026

https://insightjournals.org/pgcontent.php?jid=5&pg=About%20AJPS

Full length Paper

Investigation of thermal, optical, and passive radiation shielding properties of bismuth ore and barium oxide–doped silica-based glass

Jibrin Suleiman Yaro[1,2*], Jamilu Ari Labaran,[1.3] Abdullahi Lawal,[4] Abdullahi Ibrahim Ode[2], Iwa Samiya James[2], Adamu Saidu[4], Abubakar Bala Madaki[3]

[1]Department of Physics, Faculty of Physical Sciences, Federal University of Lafia, Nasarawa State, Nigeria.
[2]Department of Physics, School of Physical Science, Federal University of Technology Owerri, Imo State, Nigeria.
[3]Isa Mustapha Agwai Polytechnic Lafia, Nasarawa State, Nigeria.
[4]Department of Chemistry, School of Physical Science, Federal University of Technology Owerri, Imo State, Nigeria.

*Corresponding author. Email: jibrinyarsuleiman@gmail.com

Received 19 May, 2025; Accepted 23 December, 2025

ABSTRACT

Common shielding materials against highly penetrating radiations like X-rays and gamma photons are concrete and aggregates made of lead. On the other hand, concrete ages and turns opaque, and lead is costly and chemically dangerous. These and other factors have fueled the ongoing quest for substitute radiation shielding materials, and glasses have been produced with success. Mineral ores containing glass sand and bismuth ore have been generated by small-scale mining in Nigeria. Analysis of the ore found that 85.20% of the bismuth ore ($Bi_2O_2CO_3$) and glass sand was constituted of 78.99% silica. The novel glass series was made from silica derived from glass sand and included bismutite and barium oxide as dopants to alter the desired properties of the glass. With the empirical chemical formula (100-y){85[25(glass sand)+35B2O3+40Na2CO3]+15BaO}y[Bi2O2CO3], where 5≤y≥25 wt.%. The glass series was created via the melt quenching process. Measurements of optical characteristics, X-ray attenuation, and thermal analysis of the glass systems were used to characterize the new glass. The glass system has refractive index values of 2.23-2.49. The produced glass was thermally stable. All glass samples were subjected to the X-ray attenuation experiment of radiation shielding parameters, specifically the linear attenuation coefficient (LAC), mass attenuation coefficient (MAC), half value layer (HVL), and tenth value layer (TVL), at photon energies ranging from 40 to 80 kVp. The results indicate that the LAC and MAC of the glass samples decrease and increase as the photon energies increase from 40 to 80 kVp, while TVL and HVL increase and decrease as the photon energy increases (tube voltage). It is shown that the innovative glasses have higher performance in radiation shielding.

Keywords: Barium Oxide, bismutite, glass sand, optical, radiation shielding parameters, TGA and X-rays Radiation.

INTRODUCTION

In both therapeutic and diagnostic medicine, ionizing radiation has been employed more and more. However, ionizing radiation exposure can have negative effects on humans, which can be harmful to both patients and medical professionals. Therefore, in establishments that handle radiation sources, radiation protection regulations must be enforced. The management and use of radiation sources in hospitals and other businesses are governed by rules and regulations that have been promoted by nations all over the world (Acevedo-Del-Castillo et al.,

2021; Sekimoto and Katoh, 2015; Thomas and Symonds, 2016).

Radiation sickness, tumors, transmutation, and even death are some of the consequences of radiation exposure. It is clear that this is one of the most significant issues requiring the implementation of passive shields to reduce radiation exposure in order to safeguard hospital staff and patients (Deepty et al., 2019; Al-Buriahi et al., 2020; Obaid et al., 2018).

The science and practice of minimizing damage to people and the environment from ionizing radiation is known as radiation shielding. The biggest unknown when establishing nuclear power plants is radiation exposure, which calls for the use of robust radioisotopes, such as food preservation, tumor management, particle accelerator services, and diagnostic methods to stop radiation from harming staff and patients (Manohara et al., 2009; Peng et al., 2014; Kolanoski and Wermes, 2020; Rammah et al., 2021). To safeguard patients and staff, radiography institutions have incorporated a variety of safety equipment (Acevedo-Del-Castillo et al., 2021; Mostafa et al., 2020; IAEA, 2019; Sarachai et al., 2018).

Because of its high atomic number (Z), high density, high stability, and ease of processing, lead is one of the key shielding materials utilized in the creation of radiation shielding glass. However, lead is one of the main carcinogens, and its toxicity damages the ecosystem. Therefore, attempts are being made to substitute lead with other high atomic number metals in the manufacture of shielding glasses (Baptista Neto and Faria, 2014; Deepty et al., 2019; Sarachai et al., 2018; Singh et al., 2008). However, a thorough review of the literature showed that glass sand, bismuth clayey (ore), and barium oxide-based glasses have not yet been thoroughly studied as possible substitutes for lead-based glasses in radiation shielding. Despite having a reduced effective density, these substitute materials are frequently effective shields (Gaikwad et al., 2018).

As a result, medical diagnostic and treatment procedures could be hazardous to health. Lead (Pb)-based glasses are well-known and frequently used in analytical and medicinal applications due to their X-ray-defending capability to attenuate and absorb numerous varieties of photon energies (Kurudirek, 2017). High-density concrete can also be used to attenuate and absorb radiation; however, when concrete is exposed to moisture, it affects the strength and durability of the concrete, which may create a pathway for easy radiation exposure to a human being. Due to environmental concerns regarding the toxicity of lead concrete, other elements, such as glass sand (silica), bismuth ore (bismutite), and barium oxide, were used because of their low cost, durability, static, transparency, heat resistance, breakage resistance, and chemical resistance to replace lead to produce radiation shielding glasses (Singh et al., 2008).

The objectives of this paper are to synthesize (100-y){85[25(glass sand)+35H_3BO_3+40Na_2CO_3]+15BaO}y[$Bi_2(CO_3)O_2$] of the glass system, analyze the glass system's thermal and optical properties, and estimate the radiation shielding properties (HVL, LAC, MAC) of the glass system experimentally using a gamma source point. This work aims to fabricate and study the thermal, optical, and radiation shielding efficiency of the new glass series.

MATERIALS AND METHODS

Glass fabrication

A series of glasses with the chemical formula ((100-y){85[25(glass sand)+35H_3BO_3+40Na_2CO_3]+15BaO}y[$Bi_2(CO_3)O_2$]), where y is the weight percentage (y= 5, 10, 15, 20, 25%) of bismuth clayey dopant in the glass matrix, was fabricated by using a melt-quenching method as showed in Figure 1. Powdered glass sand was the source of silica in this chemical composition.

The powdered samples were weighed based on the proportion in the empirical chemical formulas using an electronic balance by Adam PW 184 with serial number (180x0.0001g) AE437713. The weighed chemicals were then mixed and stirred for about 30 minutes in a clean alumina crucible to get a homogeneous mixture (Elmahroug et al., 2018; Gaikwad et al., 2018; Naseer et al., 2021). The mixture was then preheated at 400°C for 1 hour to remove moisture, particularly because of the hygroscopic B_2O_3 (Abdul Aziz et al., 2015; Eevon et al., 2018). The preheated mixture was immediately transferred to another furnace for melting at 930°C for two hours. After melting, the molten glass was cast into a preheated mold before it was then annealed at 450°C for at least one hour in order to remove thermal stress and bubbles (Saad Aliyu et al., 2018; Naseer et al., 2021). Finally, the thickness of the glass was measured using a digital digimatic vernier caliper with model number HPM. After cutting and measuring the glasses, the glasses were then polished using a smooth-surface silicon carbide paper (6 cm x 2 cm) to give the glasses a mirror finish (Naseer et al., 2021).

X-ray radiation shielding measurement

The experimental measurement of X-ray radiation attenuation of the new glass systems was investigated to ascertain shielding effectiveness. The workroom was mounted with a digital X-ray machine; quality control was carried out to measure the output replicability, peak kilovoltage precision, and peak kilovoltage replicability. The space distance between the glass samples and x-ray tube was 45 cm, and the distance between the sources (tube voltage) and a detector window was kept at 100

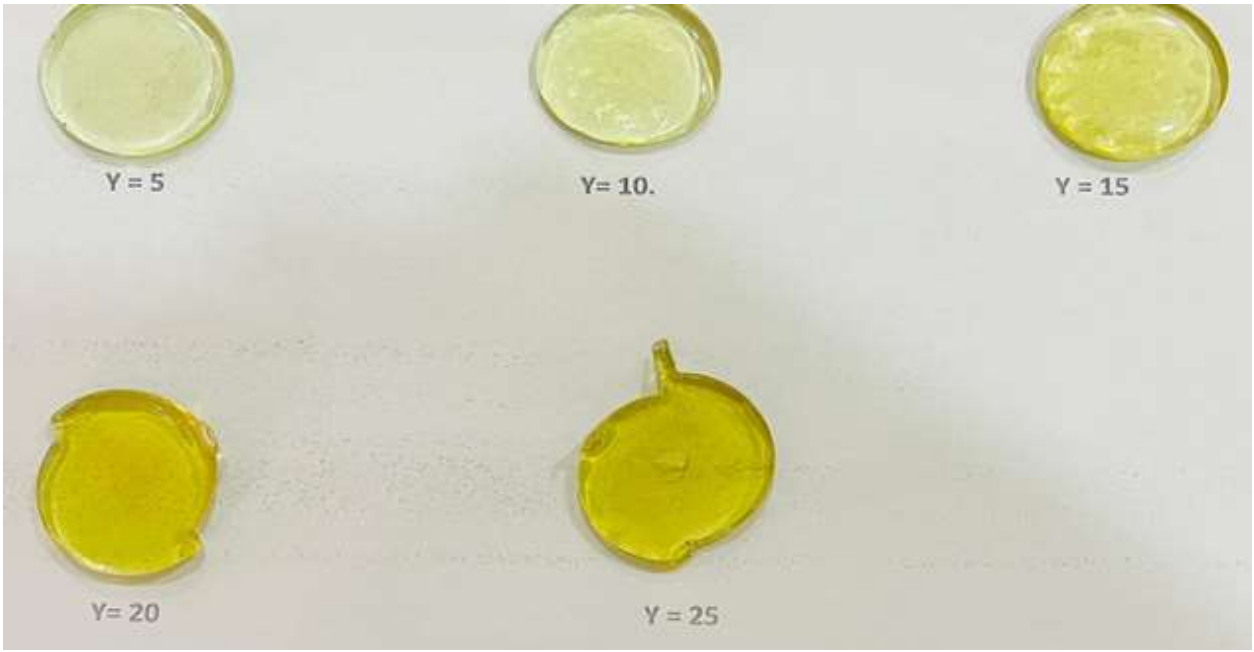

Figure 1. Composition for y = 5,10,15,20 and 25 with empirical formula (100-y){85[25(glass sand)+35H_3BO_3+40Na_2CO_3]+15BaO}y[$Bi_2(CO_3)O_2$] of the glass system.

cm. The exposure of the glasses was carried out at a fixed tube current of 20 mAs, while the tube voltage was varied from 40, 50, 60, 70, and 80 kVp. The Geiger-Mueller counter was used as the detector with a serial number of GCA-07, model number GCA-07W, with an effective diameter of 1.5-2.0 mg/cm². The detector displays dose rates in millisievert per hour (mSv/hr) ranging from 0.0005 mSv/hr to 10.0 mSv/hr (Suparta *et al*., 2014; Susoy et al., 2020). The setup of the X- The geometry of the experiment is presented in Figure 2.

Thermo Gravimetric Analysis (TGA) of the synthesized glasses

A thermal analytical technique called thermogravimetric analysis (TGA) is used to characterize substances based on their weight loss. It is a method for calculating a sample's weight in relation to temperature. With TGA, the sample is heated to a consistent temperature in a regulated setting, and the weight change is tracked over time. TGA provides a distinct picture of the analyte's makeup. Measuring weight growth or loss at a steady heating rate is the primary goal. Actually, the evaporation, oxidation, and breakdown of the analyte cause these weight variations.

The sample is put on an ultra-microbalance in a controlled environment in a thermal gravimetric analyzer. Because it provides exact measurements using coupled thermocouples, the balance is regarded as the central component of TGA. The changes that take place during thermal examination are determined by the thermocouple (Abbas, 2023).

Refractive index of the synthesized glasses

Refractive index is the measurement of how light propagates through a material. The higher the refractive index, the slower light travels through a material that changes its direction. It is a function of the material's electric permittivity and magnetic permeability, which also affects light speed (Saad Aliyu et al., 2018). In glass sciences, the refractive index (n) is defined mathematically as a function of the optical energy band gap (Eopt) as reported by Eevon et al. (2016).

$$n = \frac{n^2-1}{n^2+2} = 1-\sqrt{\frac{E_{opt}}{20}} \quad (1)$$

Where n is the refractive index, Eopt is the optical energy band gap of the glass system.

The linear attenuation coefficient μ (cm^{-1})

Linear attenuation coefficient (μ) is the percentage of photons extracted from a single energetic X-ray or gamma-ray beam per unit thickness of the material (Kara et al., 2020). Beer-Lambert's law states that as the beam travels through the material, its intensity will be reduced.

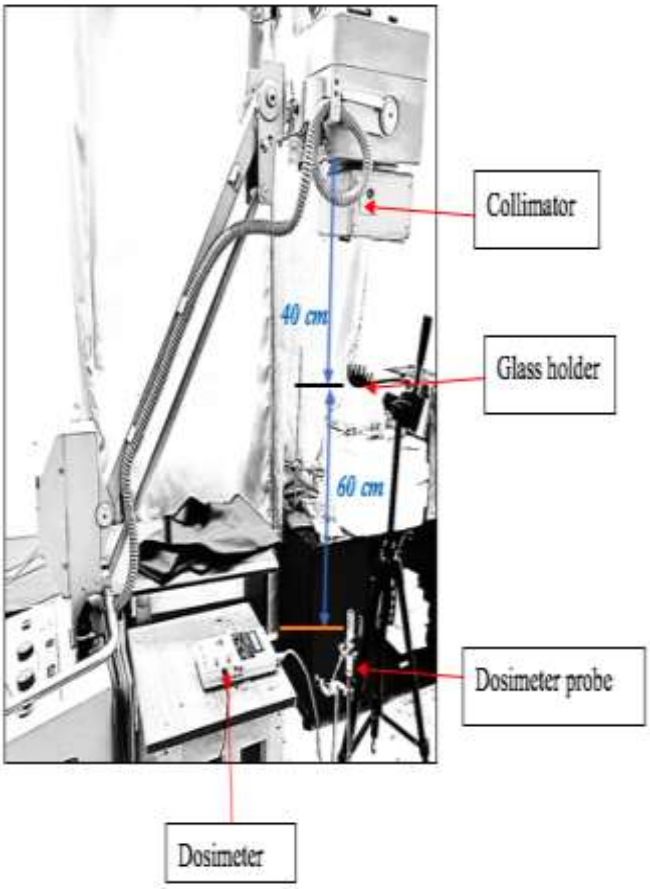

Figure 2. X-ray Experimental set-up.

$$I = I_o e^{-\mu x} \quad (2)$$

I = the intensity of photons transmitted across some distance X
IO = the initial intensity of photons.
μ = the linear attenuation coefficient
X = the thickness of the material

Half Value Layer (HVL)

The half-value layer is defined as the thickness of the absorbing material that lowers the beam's intensity to half of its initial magnitude. The better the radiation shielding property in terms of thickness needed, the lower the HVL value (Kara et al., 2020). Half-value layer is calculated by the relation given below.

$$HVL = ln\frac{2}{\mu} = \frac{0693}{\mu} \quad (3)$$

Where μ is the linear attenuation coefficient

Mean Free Path (MFP)

The mean free path is the average distance a photon may travel through a substance before interacting (Sekimoto and Katoh, 2015). The relation has calculated the mean free path from the linear attenuation coefficient (μ).

$$\mathrm{MFP} = \frac{1}{\mu} \quad (4)$$

RESULTS AND DISCUSSION

Characterizations of bismutite and glass sand ores

Energy Dispersive X-ray Fluorescence (EDXRF) revealed the two ores contain ~60 wt % Bi and ~78.96 wt % Si, which denotes Bi-O and The Bi ore contained C, O, V,

Table 1. Chemical Constituent in the Glass Sand Collected Shabu, Lafia LGA**.**

	Amount /percentage (%)	
Element (Oxide)	**Raw result**	**Normalized result**
Fe_2O_3	0.6139	0.698
SiO_2	78.963	89.738
AL_2O_3	4.825	5.483
MgO	1.45	1.648
P_2O_5	0.2755	0.313
K_2O	0.6736	0.766
SrO	0.368	0.418
Nb_2O_5	0.1249	0.142
Bi_2O_3	0.2252	0.256
BaO	0.4738	0.538

Table 2. Refractive Index of the glass system

Bismutite=Y (wt. %)	Refractive Index (n)
5	2.23
10	2.49
15	2.31
20	2.32
25	2.34

Cu, Al, and Si, while the glass sand sample's metallic oxides are presented in Table 1.

In Table 1 the EDXRF revealed that the glass sand contains 89.738% silica, which is needed as a glass former, and some traces of metallic oxide impurities.

Optical and thermal properties of the glasses

As the ($Bi_2(CO_3)O_2$) concentration increased from 5 to 25 weight percent, the fabricated glasses were investigated. The results of the refractive index (n) of the glasses, which was computed using Equation 4, are presented in Table 2. As observed, the refractive index increased from 2.23 to 2.49, decreased from 2.49 to 2.31, and then increased from 2.31 to 2.34. The increase in the refractive index may be related to a change in the structural arrangements of the atoms in the glass network, as shown in Figure 3.

Figure 3 shows the refractive index of the glasses. The results revealed that the refractive index of the fabricated glasses increased from 2.23 to 2.49, decreased from 2.49 to 2.31, and then increased from 2.31 to 2.34. The increase in the refractive index may be related to a change in the structural arrangements of the atoms in the glass network that produces more NBO, which increased the polarizability of the material through the increase in the NBOs produced. NBOs are more polarizable than bridging oxygen (BOs) (Eevon et al., 2016).

Thermal analysis of the synthesized glasses

To determine how well the glasses worked for their thermal stability, a thermal examination of the glass samples was done. Figure 4 displays the thermogram of the TGA result for the glass samples with a few various temperatures, such as the melting temperature (Tm), the initial temperature (Ti), and the final temperature (Tf). Additional metrics, including mass weight change and glass forming ability (Tgf), can be utilized to determine the useful application of the glass system. A greater resistance to thermal damage from the external environment is indicated by a higher Ti value (Abbas, 2023; Alam and Mohammad, 2021; Peng et al., 2014). According to Soltan et al. (2013), the glass's high temperature stability suggests a robust reserve of manifestation and nucleation within the glass structure. The glass system's thermal stability for different weight percentages, with temperatures ranging from 200°C to 180°C, respectively, is observed. This indicates that the prepared glass system has a higher thermal stability and a more straightforward formation. According to Paz et al. (2016), glass that exhibits thermal stability above 100°C is both good for fiber drawing and stable against devitrification.

X-Ray radiation shielding properties of glass samples

The glass samples produced were exposed to an X-ray beam in order to ascertain the radiation shielding ability of the glass. The data on the linear attenuation coefficient (LAC) is presented in Table 3. The result revealed that the LAC of all the glass samples decreases with the increasing of photon energy (or tube voltage) ranging from 40 kVp to 80 kVp. However, the results indicate higher penetration of X-rays was observed at high photon energy.

Table 3 shows that the linear attenuation coefficient is higher at 20 wt.% concentration of bismuth clayey (50,

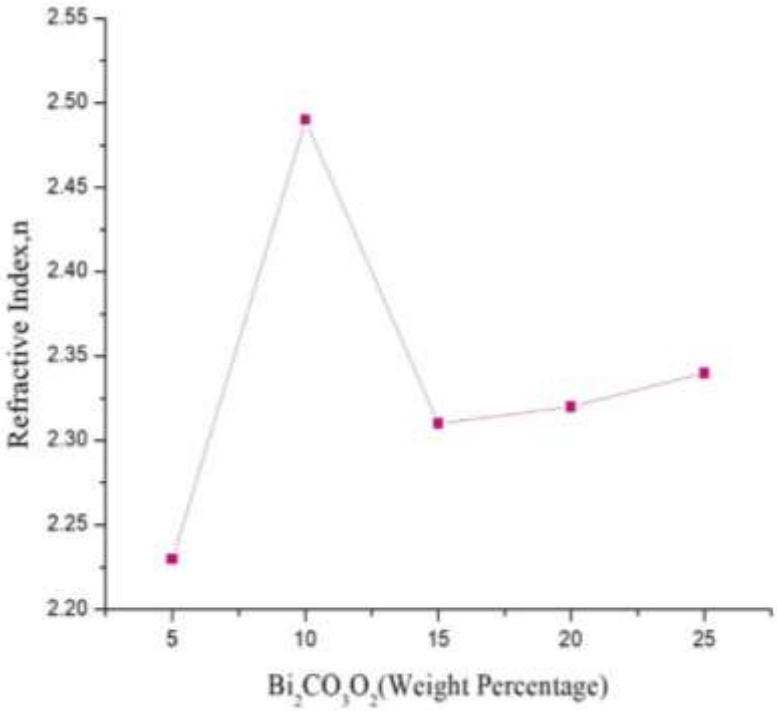

Figure 3. Refractive index *of the* synthesized glasses against weight percentage of Bismuth ore (Bismutite).

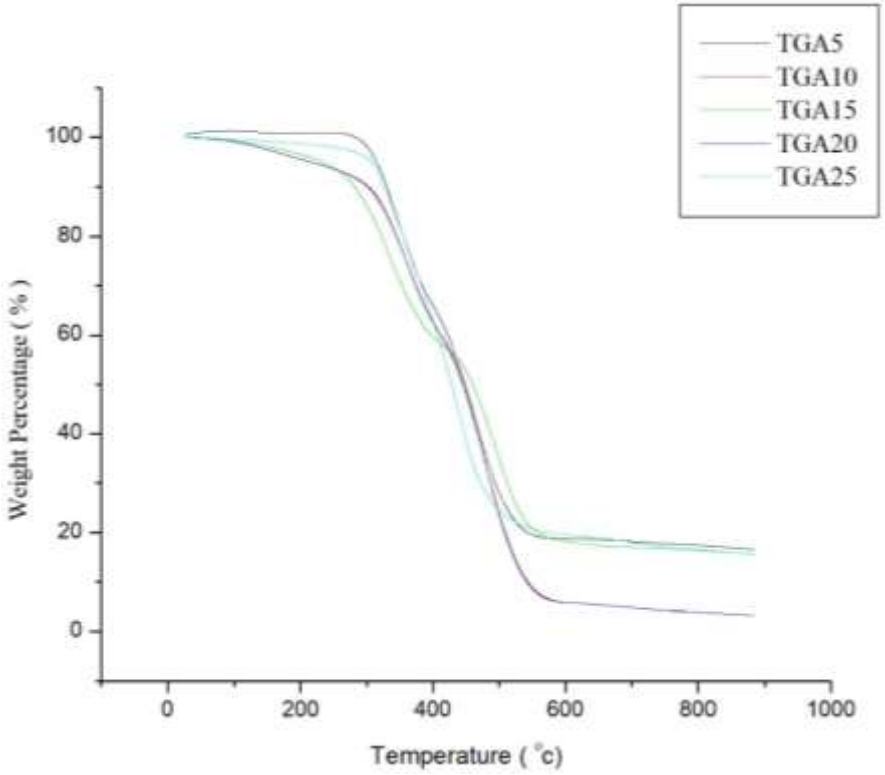

Figure 4. TGA for (100-y){85[25(glass sand)+35H_3BO_3+40Na_2CO_3]+15BaO}y[$Bi_2O_2CO_3$)] of the glass system.

Table 3. LAC of Glass Samples at different photon energy

Photon energy (kVp)	GLS5	GLS10	GLS15	GLS20	GLS25
40	6.41	10.68	14.96	16.87	17.32
50	6.29	6.98	11.71	14.08	13.43
60	2.49	2.74	4.86	8.30	8.07
70	3.36	1.85	3.58	5.60	4.85
80	1.26	1.15	1.96	2.47	1.85

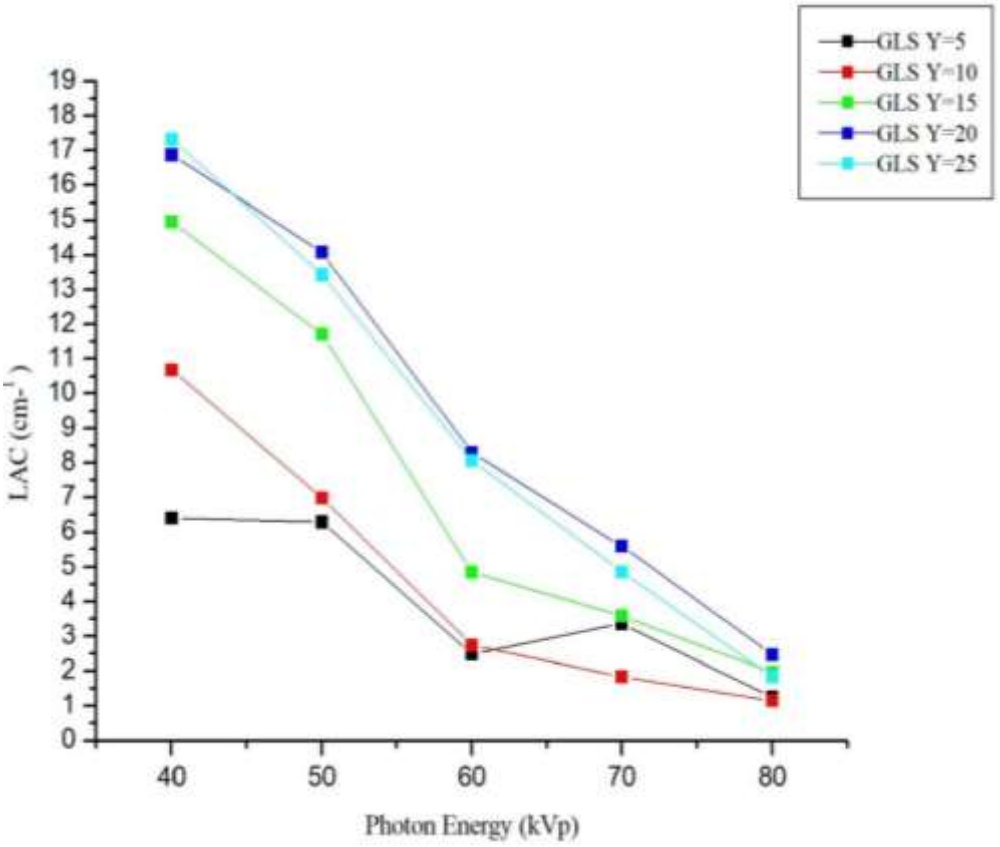

Figure 5. Linear attenuation coefficient of fabricated glass systems.

60, 70, and 80 kVp), while 25 wt.% of bismuth ore (bismutite) has the highest LAC at 40 kVp. However, LAC is minimum at 40, 50, and 60 kVp of 0.5 wt.% $Bi_2O_2CO_3$ Also, the least LAC was observed at 10 wt.% $Bi_2O_2CO_3$.

Figure 5 shows that the higher the tube voltage, the higher the penetration. It was established that the glass sample at 25 wt.% of bismuth ore has the highest linear attenuation coefficient values, while the glass sample at 5 wt.% of bismuth ore (bismutite) has the least LAC. Sarachai et al. (2018) reported that the glass samples fabricated are related to commercial lead glass.

Figure 6 shows that the mass attenuation coefficient is higher at 20 wt.% concentration of bismuth ore (bismutite), followed by 25 wt.%, while MAC is minimum at 05% weight. Also at lower tube voltage (40 kVp), better MAC was identified. This is in agreement with Sarachai et al. (2018).

Figure 7 presents the HVL of the glass samples against photon energy (kVp). The results show that the half-value layer values of the glass samples at kVp 40, 50, and 60 of GLS5 are higher than all the samples, followed by GLS10, while sample GLS20 has the least half-value

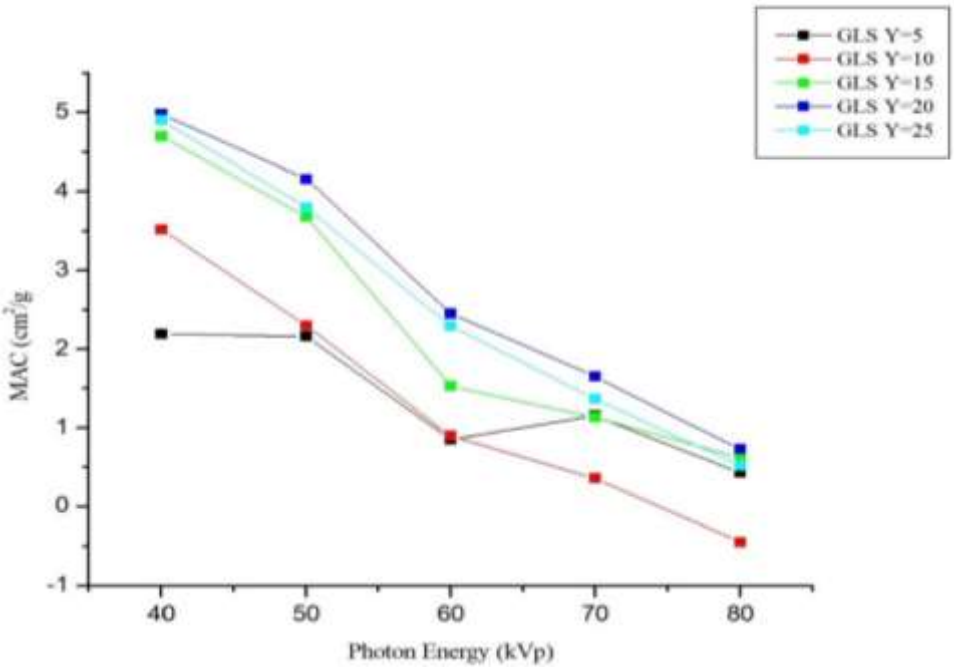

Figure 6. Mass Attenuation Coefficient of the fabricated glass.

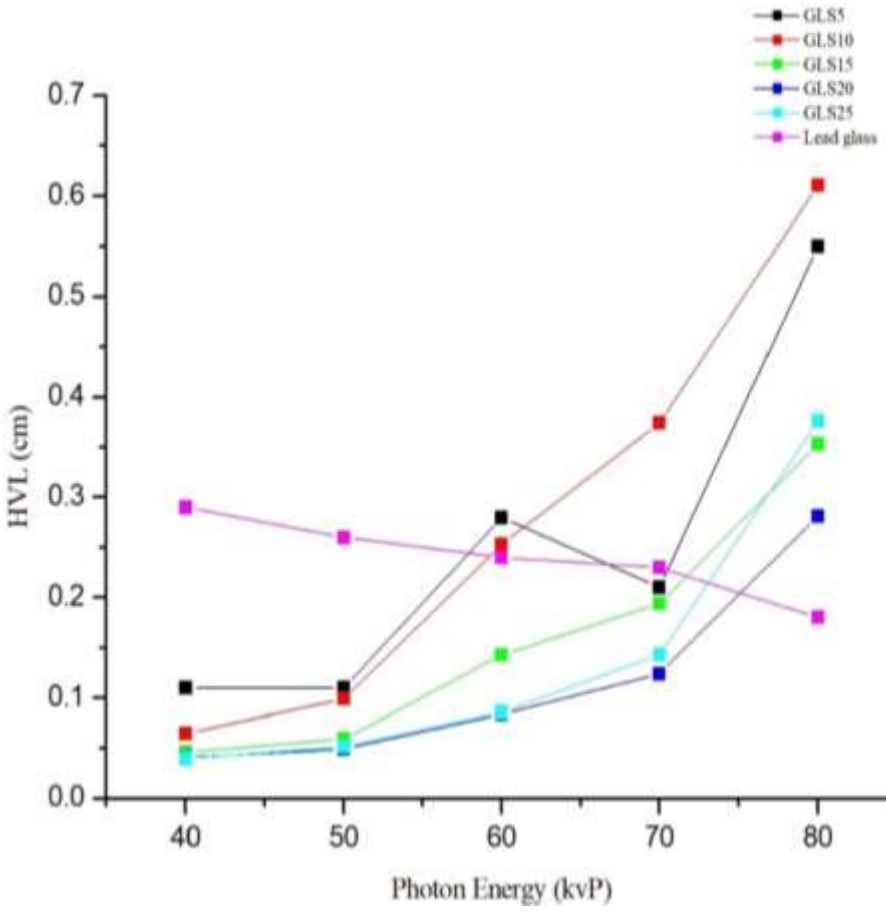

Figure 7. Half Value Layer of glass system.

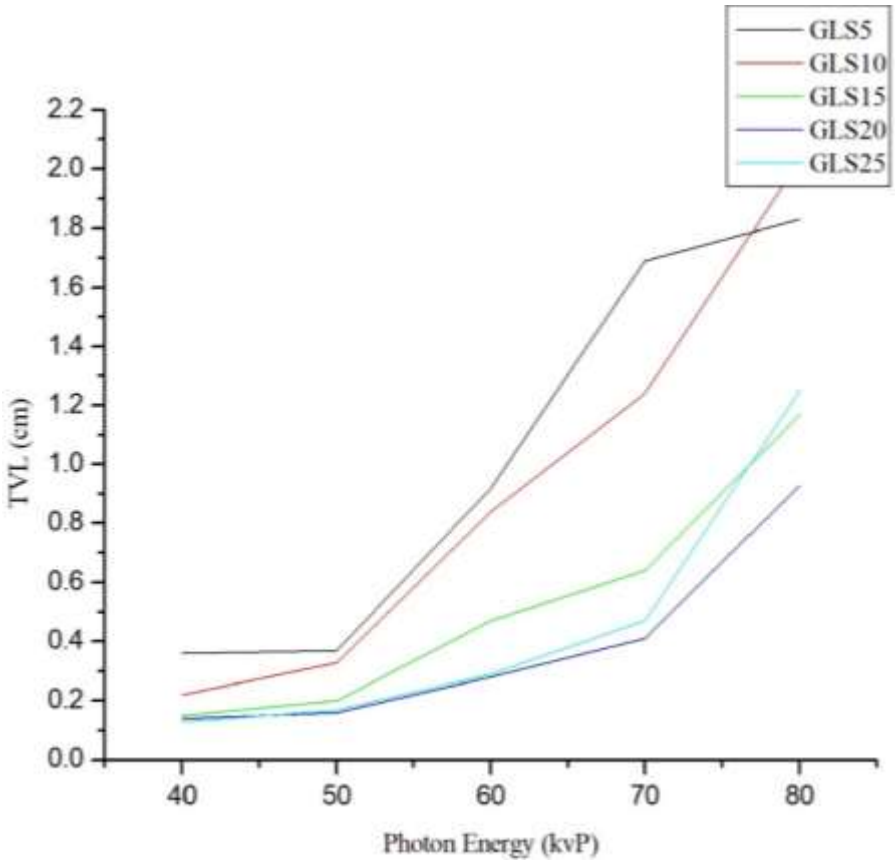

Figure 8. Tenth Value Layer of glass system.

layer. Hence, kVp at 80 has the highest HVL. This revealed that GLS20 will attenuate better irrespective of the photon energy (kVp).

Sarachai et al. (2018) reported the same affirmation in Figure 8. It was established that the HVL values of the glass samples at 20 wt.% of bismuth ore (bismutite) are lower than commercial lead glass, while commercial lead glass is lower than the produced glasses at 70 and 80 kVp. However, all the glass samples produced attenuate better at 40 kVp. It is shown that the innovative glasses have higher performance in radiation shielding.

The results depict that GLS20 has the lowest tenth value layer at all photon energy (kVp), then GLS25, while GLS5 at 40, 50, 60, and 70 kVp has the highest TVL. So also, GLS10 at 80 kVp has higher TVL. However, the figure revealed a similar trend to that of HVL.

CONCLUSION

Using the melt quench process, glass sand ore doped with bismutite and barium oxide with a chemical composition of (100-y) 85[25 (glass sand)-35B_2O_3-40Na_2CO_3)15BaOy, y = 5, 10, 15, 20, and 25 weight percentage, was fabricated. The glass sand's silica content was confirmed to be 78.99% by the X-ray fluorescence (DEXRF) result. The glass system has a refractive index value between 2.23 and 2.49. The fabricated glasses are thermally stable. The linear attenuation coefficient of every glass sample rose as $Bi_2O_2CO_3$ concentrations rose and decreased as photon energy increased between 40 and 80 kVp, according to X-ray attenuation measurements. 20% weight of $Bi_2O_2CO_3$ has a greater mass attenuation coefficient, whereas the least mass attenuation coefficient was observed at 05%. Also at lower tube voltage (40 kVp), better MAC was identified. Thus, MAC and LAC displayed the same behavior. GLS5 outperforms all other samples at 40, 50, and 60 kVp, followed by GLS10, and sample GLS20 has the lowest half value layer, according to the glass samples' half value layer values. So, the maximum HVL is found in 80 kVp. Regardless of the photon energy (kVp), GLS20 will attenuate more effectively, according to this. The results indicated that the mean free path from all indications demonstrated similar steps to those for the half-value layer when comparing the mean free path with the kVp and the $Bi_2O_2CO_3$. With HVL and MFP, TVL found a similar trend. The manufactured glass samples are connected to commercial lead glass, according to Kamislioglu (2021).

ACKNOWLEDGEMENT

We wish to acknowledge everyone at the Muhammadu Buhari Research Center, Federal University of Lafia, Nasarawa State, for providing the space and technical assistance that allowed this research to be conducted.

CONFLICT OF INTEREST

The authors declare no conflicts of interest.

REFERENCES

Abbas, B. (2023). *Thermogravimetric analysis (TGA)*. Definitive Guide. Pp. 214-223.

Abdul Aziz, S. H., El-Mallawany, R., Badaron, S. S., Kamari, H. M., and Amin Matori, K. (2015). Optical properties of erbium zinc tellurite glass system. *Advances in Materials Science and Engineering, 1*: 628954.

Acevedo-Del-Castillo, A., Águila-Toledo, E., MaldonadoMagnere, S., and Aguilar-Bolados, H. (2021). A brief review on the high-energy electromagnetic radiation-shielding materials based on polymer nanocomposites. *International journal of molecular sciences*, *22*(16), 9079.

Alam, S., and Chowdhury, M. A. (2021). Thermal gravimetric analysis of glass fiber reinforced composite for understanding the impact of copper oxide in relation to titanium oxide filler particles. *Composites Theory and Practice*, 21(1-2): 12-21.

Al-Buriahi, M. S., Rashad, M., Alalawi, A., and Sayyed, M. I. (2020). Effect of Bi2O3 on mechanical features and radiation shielding properties of boro-tellurite glass system. *Ceramics International*, *46*(10):16452-16458.

Baptista Neto, A. T., and Faria, L. O. (2014). Construction and Calibration of a multipurpose instrument to simultaneously measure dose, voltage and half-valuelayer in X-ray emission equipment. *Radiation Measurements*, *71:* 178-182.

Deepty, M., Srinivas, C., Kumar, E. R., Mohan, N. K., Prajapat, C. L., Rao, T. V. C., Meena, S. S., Verma, A. K., and Sastry, D. L. (2019). XRD, EDX, FTIR and ESR Spectroscopic Studies of Co-precipitated Mn–substituted Zn–ferrite nanoparticles. *Ceramics International*, *45*(6): 8037-8044.

Eevon, C., Halimah, M. K., Zakaria, A., Azurahanim, C. A. C., Azlan, M. N., and Faznny, M. F. (2016). Linear and nonlinear optical properties of Gd^{3+} doped zinc borotellurite glasses for all-optical switching applications. *Results in Physics*, *6:* 761766.

Elmahroug, Y., Almatari, M., Dong, M., and Tekin, H. O. (2018). Investigation of radiation shielding properties for Bi_2O_3 - V_2O_5 -TeO_2 glass system using MCNP5 code. *Journal of Non-Crystalline Solids*, *499:* 32-40.

Gaikwad, D. K., Obaid, S. S., Sayyed, M. I., Bhosale, R. R., Awasarmol, V. V., Kumar, A., Shirsat, M. D., and Pawar, P. P. (2018). Comparative study of gamma ray shielding competence of WO3-TeO2-PbO glass system to different glasses and concretes. *Materials Chemistry and Physics*, *213*: 508-517.

IAEA (2019). Postgraduate Education Course in Radiation Protection and Safety of Radiation Sources: Standard Syllabus. *Training Course Series*, *18*, 12-14.

Kaewjaeng, S., Boonyu, K., Kim, H. J., Kaewkhao, J., and Kothan, S. (2020). Study on radiation shielding properties of glass samples doped with holmium. In *AIP Conference Proceedings* (Vol. 2279, No. 1, p. 060005). AIP Publishing LLC.

Kamislioglu, M. (2021). Research on the effects of bismuth borate glass system on nuclear radiation shielding parameters. *Results in Physics*, *22*:103844.

Kara, U., Kavaz, E., Issa, S. A., Rashad, M., Susoy, G., Mostafa, A. M. A., Yildiz Yorgun, N. and Tekin, H. O. (2020). Optical, structural and nuclear radiation shielding properties of Li2B4O7 glasses: effect of boron mineral additive. *Applied Physics A,* 126(4): 261. https://doi.org/10.1007/s00339-020-3397-8.

Kurudirek, M. (2017). Heavy Metal Borate Glasses: Potential use for Radiation Shielding. *Journal of Alloys and Compounds, 727:* 1227-1236.

Manohara, S. R., Hanagodimath, S. M., and Gerward, L. (2009). Photon interaction and energy absorption in glass: A transparent gamma ray shield. *Journal of Nuclear Materials*, *393*(3): 465-472.

Mostafa, A. M. A., Zakaly, H. M. H., Pyshkina, M., Issa, S. A. M., Tekin, H. O., Sidek, H. A. A., Matori, K. A., and Zaid, M. H. M. (2020). Multi-objective optimization strategies for radiation shielding performance of BZBB glasses using Bi_2O_3: A FLUKA Monte Carlo code calculations. *Journal of Materials Research and Technology*, *9*(6): 12335-12345.

Naseer, K. A., Marimuthu, K., Mahmoud, K. A., and Sayyed, M. I. (2021). Impact of Bi_2O_3 modifier concentration on bariumzincborate glasses: physical, structural, elastic, and radiationshielding properties. *European Physical Journal Plus*, *136:* 116.

Obaid, S. S., Gaikwad, D. K., and Pawar, P. P. (2018). Determination of gamma ray shielding parameters of rocks and concrete. *Radiation Physics and Chemistry*, *144:* 356-360.

Paz, E. C., Dias, J. D. M., Melo, G. H. A., Lodi, T. A., Carvalho, J. O., Façanha Filho, P. F., Barboza, M. J., Pedrochi, F., and Steimacher, A. (2016). Physical, thermal and structural properties of calcium borotellurite glass system. *Materials Chemistry and Physics, 178:* 133-138.

Peng, S., Yang, F., Wu, L., Qi, Y., Zheng, S., Yin, D., Wang, X. and Zhou, Y. (2014). Multicolor upconversion emission and energy transfer mechanism in Er^{3+}/Tm_3+/Yb_3+ codoped tellurite glasses. *Journal of Quantitative Spectroscopy and Radiative Transfer,* 147: 155-63.

Rammah, Y. S., EL-Agawany, F. I., Gamal, A., Olarinoye, I. O., Ahmed, E. M., & Abuohaswa, A. S. (2021). Responsibility of Bi_2O_3 content in photon, alpha, proton, fast and thermal neutron shielding capacity and elastic moduli of zinc/B_2O_3/Bi_2O_3 glasses. *Journal of Inorganic and Organometallic Polymers and Materials, 31*(8): 3505-3524.

Saad Aliyu, U., Mohamed Kamari, H., Muhammad Hamza, A., and Abdulla Awshah, A. (2018). The Structural, Physical and Optical Properties of Borotellurite Glasses Incorporated with Silica from Rice Husk. *Journal of Science and Mathematics Letters*, *6*, 32-46.

Sarachai, S., Chanthima, N., Sangwaranatee, N. W., Kothan, S., Kaewjaeng, S., Tungjai, M., Djamal, M., and Kaewkhao, J. (2018). Radiation shielding properties of BaO-ZnO-B_2O_3 glass for X-ray room. *Key Engineering Materials*, *766:* 88-93.

Sekimoto, M., and Katoh, Y. (2015). Coloring characteristic of lead glass for X-ray irradiation. *New Journal of Glass and Ceramics*, *5*(3): 25-30.

Singh, S., Kumar, A., Singh, D., Thind, K. S., and Mudahar, G.

S. (2008). Barium–borate–flyash glasses: as radiation shielding materials. *Nuclear Instruments and Methods in Physics Research Section B: Beam Interactions with Materials and Atoms*, *266*(1): 140-146.

Soltan, A. S., Abu-Sehly, A. A. Joraid, A. A and. Alamri, S. N. (2013). The activation energy and fragility index of the glass transition in Se76Te21Sb3 chalcogenide glass. *Thermochimica Acta,* 574: 73-78.

Susoy, G., Guclu, E. A., Kilicoglu, O., Kamislioglu, M., Al-Buriahi, M. S., Abuzaid, M. M., and Tekin, H. O. (2020). The impact of Cr_2O_3 additive on nuclear radiation shielding properties of LiF–SrO–B_2O_3 glass system. Materials Chemistry and Physics, 242: 122481. https://doi.org/10.1016/j.matchemphys.2019.12248

Suparta, G. B., Louk, A. C., Sam, N. H., and Wiguna, G. A. (2014). Quality performance of customized and low cost x-ray micro-digital radiography system. In *International Conference on Experimental Mechanics 2013 and Twelfth Asian Conference on Experimental Mechanics* 9234: 239245). SPIE.

Thomas, G. A., and Symonds, P. (2016). Radiation exposure and health effects - Is it time to reassess the real consequences? *Clinical Oncology*, *28*(4): 231-236.